

See discussions, stats, and author profiles for this publication at: <https://www.researchgate.net/publication/262929551>

# The Importance of Large-Amplitude Motions for the Interpretation of Mid-Infrared Vibrational Absorption and Circular Dichroism Spectra: 6,6'-Dibromo-[1,1'-binaphthalene]-2,2'-di...

ARTICLE *in* THE JOURNAL OF PHYSICAL CHEMISTRY A · JUNE 2014

Impact Factor: 2.69 · DOI: 10.1021/jp4114738 · Source: PubMed

---

CITATIONS

3

---

READS

33

## 4 AUTHORS, INCLUDING:



Mojgan Heshmat

VU University Amsterdam

8 PUBLICATIONS 50 CITATIONS

[SEE PROFILE](#)



Evert Jan Baerends

VU University Amsterdam

481 PUBLICATIONS 39,255 CITATIONS

[SEE PROFILE](#)

# The Importance of Large-Amplitude Motions for the Interpretation of Mid-Infrared Vibrational Absorption and Circular Dichroism Spectra: 6,6'-Dibromo-[1,1'-binaphthalene]-2,2'-diol in Dimethyl Sulfoxide

Mojgan Heshmat,<sup>†</sup> Evert Jan Baerends,<sup>†,‡,§</sup> Prasad L. Polavarapu,<sup>||</sup> and Valentin Paul Nicu\*,<sup>†</sup>

<sup>†</sup>Department of Chemistry, VU University Amsterdam, De Boelelaan 1083, 1081 HV Amsterdam, The Netherlands

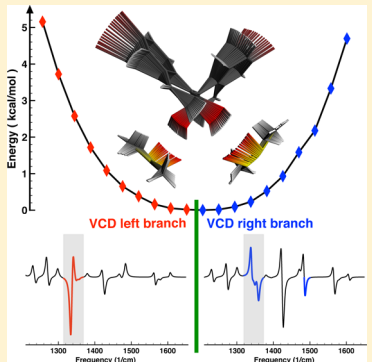
<sup>‡</sup>WCU program, Department of Chemistry, Pohang University of Science and Technology, San 31, Hyojadong, Namgu, Pohang 790-784, South Korea

<sup>§</sup>Chemistry Department, Faculty of Science, King Abdulaziz University, Jeddah 21589, Saudi-Arabia

<sup>||</sup>Department of Chemistry, Vanderbilt University, Nashville, Tennessee 37235, United States

## S Supporting Information

**ABSTRACT:** Using the 6,6'-dibromo-[1,1'-binaphthalene]-2,2'-diol molecule and its vibrational absorption (VA) and vibrational circular dichroism (VCD) spectra measured in deuterated dimethyl sulfoxide as example, we present a first detailed study of the effects induced in VCD spectra by the large-amplitude motions of solvent molecules loosely bound to a solute molecule. We show that this type of perturbation can induce significant effects in the VA and VCD spectra. We also outline a computational procedure that can effectively model the effects induced in the spectra and at the same time provide detailed structural information regarding the relative orientations of moieties involved in a solute–solvent molecular complex.



## 1. INTRODUCTION

The increasingly high demand for single enantiomeric molecular compounds in the pharmaceutical industry has made asymmetric catalysis a very important and active research direction in chemistry.<sup>1–4</sup> A common challenge encountered when one tries to elucidate the mechanisms behind any asymmetric synthesis in solution is to understand the role played by the solvent.<sup>5–7</sup> Vibrational circular dichroism (VCD) spectroscopy has the potential to provide valuable information for this purpose, as VCD spectra are extremely sensitive to molecular conformations<sup>8–10</sup> and also to intermolecular hydrogen bond formation between solute and solvent molecules.<sup>11–20</sup>

As a first study in this direction, we have investigated in ref 10 the differences between the experimental VCD spectra of [1,1'-binaphthalene]-2,2'-diol (a well-known ligand for asymmetric catalysis<sup>21</sup>) in three different solvents, i.e., dichloromethane, deuterated acetonitrile, and deuterated dimethyl sulfoxide ( $\text{DMSO}-d_6$ ). This study has shown that the effects induced in the VCD and vibrational absorption (VA) spectra by solute–solvent molecular complex formation depend sensitively on the solvent used. This study has also shown that the observed changes in the VA and VCD spectra are caused by three main perturbations: (1) perturbation of the Boltzmann populations of the various conformers of the solute, (2)

perturbation of the normal modes of the solute, and (3) perturbation of the electronic structure of the solute.

In this work we investigate another possible source of perturbation induced by the solvent that has the potential to significantly affect the measured VCD spectra, i.e., the large-amplitude motion of solvent molecules that are loosely bound to the solute molecule. To study this particular type of perturbation, we have considered a molecule very similar to the one used in ref 10, i.e., the 6,6'-dibromo-[1,1'-binaphthalene]-2,2'-diol molecule (hereafter referred to as DBBN), and its VA and VCD spectra measured in DMSO.

In DMSO, the two O–H bonds of DBBN will form intermolecular hydrogen bonds with the DMSO solvent molecules.<sup>10</sup> Because these intermolecular hydrogen bonds are weak, and the complex is very labile, the complexing solvent molecule will carry out large-amplitude motions with respect to the solute, which are slow relative to the solute modes that appear in the mid-infrared region. To simulate the effects induced in the VA and VCD spectra by these large-amplitude motions of solvent molecules, we have systematically varied the relative orientation of the solvent and solute molecules involved

Received: November 21, 2013

Revised: June 5, 2014

Published: June 6, 2014

in the molecular complex by performing linear transit calculations (see section 4 for details). Then, we have computed vacuum and COSMO VA and VCD spectra for all structures generated during the linear transit scans.

The main goal of this work is to study the effect of the shallow nature of the solvent–solute interaction energy curves. In particular, we are interested in (1) identifying and quantifying the type of changes induced in the VA and VCD spectra computed for molecular complexes when the relative position and orientation of the solvent molecule are varied with respect to the solute, (2) assessing whether it is necessary and/or beneficial to take into account in simulation the effect of large-amplitude motions of the solvent, and (3) assessing the dielectric continuum effect of the wider solvent environment on the equilibrium values of the solute–solvent coordinates.

As will be shown, to obtain meaningful simulated spectra for the studied molecular complex (that also reproduce the experimental spectra well), it is necessary to account for these large-amplitude motions. The reason for this is 2-fold. On the one hand, the profile of the potential energy surface (PES) along the weak intermolecular hydrogen bonds is very flat. As such, standard geometry optimization calculations may lead to different “relaxed” structures for the molecular complex if one uses (1) slightly different computational parameters or (2) different starting structures for the geometry optimization calculation. On the other hand, these different “relaxed” structures can have different VCD spectra even though their energies are very similar. Consequently, instead of making predictions based on the spectra computed for a single arbitrary “relaxed” structure, it is better to average the computed spectra of all linear transit structures.

## 2. EXPERIMENTAL AND THEORETICAL DETAILS

**2.1. Experiment.** The experimental VCD spectra were measured on a commercial ChiralIR spectrometer acquired in 1998. This spectrometer was subsequently modified to accommodate a postsample photoelastic modulator and a second lock-in amplifier to reduce the artifacts.<sup>22</sup> The spectra were measured at a concentration of 16.5 mg/mL in DMSO-*d*<sub>6</sub> solvents, using 8 cm<sup>-1</sup> spectral resolution and 1 h data collection time. The samples were held in a variable path length cell with barium fluoride windows. VCD spectra were collected for both enantiomers. The presented spectra were obtained as one-half of the difference between the spectra obtained for (*R*)-(-) and (*S*)-(+) enantiomers.

**2.2. Computational Details.** All geometry optimizations (including the linear transit ones), harmonic vibrational frequencies, and VCD intensities were calculated using the ADF program package.<sup>23–26</sup> The BP86 functional<sup>27,28</sup> and a Slater type orbital (STO) basis set of triple- $\zeta$  plus polarization functions (TZP) quality<sup>29</sup> were used in all calculations.

Both vacuum and COSMO<sup>30–32</sup> calculations have been performed. In the vacuum calculations all geometry optimizations, VA and VCD calculations have been performed for the isolated molecular complex considered. In the COSMO calculations the considered molecular complex was embedded in the dielectric continuum corresponding to DMSO (dielectric constant of 46.7).

Normal-mode overlaps have been calculated using the ToolsVCD program.<sup>33</sup> The calculated VA and VCD spectra were obtained by Lorentzian broadening of the peak intensities using a half-width of 8 cm<sup>-1</sup>. The harmonic frequencies have not been scaled.

## 3. MOLECULAR STRUCTURE

As shown in Figure 1, the DBBN molecule has axial chirality and three main conformers.<sup>34,35</sup> These three conformers are labeled C<sup>1</sup>, C<sup>2</sup>, and C<sup>3</sup> and differ in the orientation of the O–H bonds.

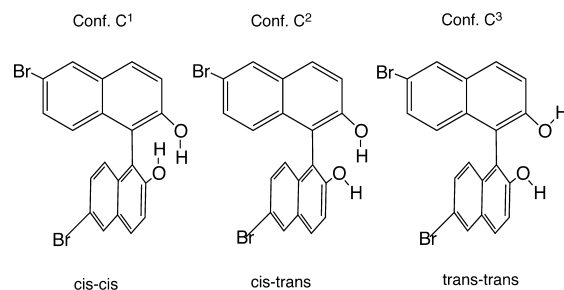


Figure 1. Schematic representation of the three conformers of DBBN.

As discussed in ref 10 (see also Figure 1 in the Supporting Information), to reproduce the experimental spectra measured in DMSO, it is necessary to perform calculations for molecular complexes formed between one DBBN and two DMSO molecules (one at each O–H bond); viz., in DMSO the two O–H bonds of DBBN form intermolecular hydrogen bonds with the solvent molecules.<sup>10</sup> Therefore, only molecular complexes formed between one DBBN and two DMSO molecules (Figure 2) have been considered in this study. Table 1 lists the relative energies and the corresponding Boltzmann weights computed for three molecular complexes (one for each conformer) at two different levels of theory, i.e., (vacuum, BP86, TZP) and (COSMO, BP86, TZP). As can be seen, both

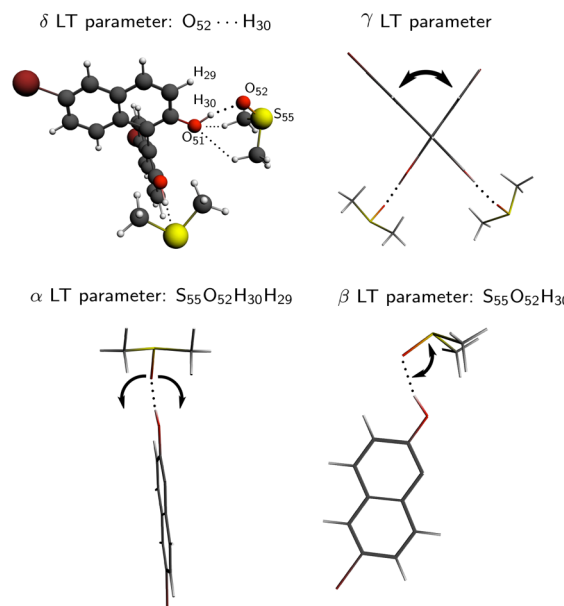


Figure 2. Linear transit parameters. The upper left panel shows a “balls and sticks” representation of the optimized (BP86, TZP, vacuum) geometry of the C<sup>3</sup>–(DMSO)<sub>2</sub> complex. The upper right panel shows the dihedral angle  $\gamma$  between the two naphthalene planes (the molecule is visualized as “sticks without balls”). The lower panel shows the  $\alpha$  dihedral angle (left) and the  $\beta$  angle (right) at one of the naphthol groups. For clarity, only one naphthol and the associated DMSO molecule (i.e., only half of the C<sup>3</sup>–(DMSO)<sub>2</sub> complex) are shown in the lower panel.

**Table 1.** Relative Energies ( $\Delta E$ ) and Boltzmann Weights (BW) Computed at (BP86, TZP, Vacuum) and (BP86, TZP, COSMO) Level of Theory for the Molecular Complexes of DBBN with DMSO<sup>a</sup>

molecular complex	vacuum		COSMO	
	$\Delta E$ (kcal/mol)	BW	$\Delta E$ (kcal/mol)	BW
$C^1-(DMSO)_2$	3.090	0.004	5.320	0.000
$C^2-(DMSO)_2$	0.740	0.222	2.850	0.008
$C^3-(DMSO)_2$	0.000	0.774	0.000	0.992

<sup>a</sup>Because DBBN has three conformers, i.e.,  $C^1$ ,  $C^2$ , and  $C^3$ , one molecular complex was considered for each conformer, i.e.,  $C^1-(DMSO)_2$ ,  $C^2-(DMSO)_2$ , and  $C^3-(DMSO)_2$ .

vacuum and COSMO calculations have predicted the molecular complex formed with conformer  $C^3$ , i.e.,  $C^3-(DMSO)_2$ , to be the dominant one.

#### 4. GEOMETRICAL DEGREES OF FREEDOM AND LARGE-AMPLITUDE MOTIONS

To account in simulation for the slow (but with large amplitude) motion of the solvent molecules with respect to the solute, the relative orientation and position of the solute and solvent molecules involved in a molecular complex was systematically varied by performing linear transit (LT) calculations. A LT calculation is performed in two steps. In the first step, a set of intermediate structures (hereafter referred to as LT structures) are generated by varying a geometrical parameter (e.g., bond length, bond angle, dihedral angle) from its initial value to a final value in a number of steps. The geometrical parameter (hereafter referred to as the LT parameter), its final value, and the number of LT steps are defined by the user in the beginning of the LT calculation. In

the second step, a constrained geometry optimization is performed for each LT structure generated in the first step; i.e., the value of the LT parameter characterizing a given LT structure is kept fixed during the geometry optimization of all other geometrical parameters.

Because both vacuum and COSMO calculations have predicted conformer  $C^3$  to be the dominant one (Table 1), the LT calculations have been performed only for the molecular complex with conformer  $C^3$ , i.e.,  $C^3-(DMSO)_2$ . The geometry of the  $C^3-(DMSO)_2$  complex used as the starting point in all LT calculations was obtained by performing a geometry optimization calculation with very tight criteria for the geometry convergence, i.e.,  $10^{-4}$  Hartree/Å for gradients and  $10^{-6}$  Hartree for energy. Starting from this geometry, we have scanned four different LT parameters (shown in Figure 2) for  $C^3-(DMSO)_2$ :

- (1)  **$\alpha$  dihedral angle.**  $\alpha$  is the dihedral angle made by the symmetry plane of a DMSO molecule and the plane of the corresponding naphthalene ring (Figure 2). It describes the tilting of a DMSO molecule with respect to the corresponding naphthalene ring. In the vacuum LT calculations  $\alpha$  was varied by  $\pm 90^\circ$  in steps of  $10^\circ$  starting from the value of  $185^\circ$ .
- (2)  **$\beta$  angle.**  $\beta$  is the angle between the S=O bond of a DMSO molecule and the adjacent intermolecular H bond between the O atom of DMSO and the H atom of the O-H bond of DBBN (Figure 2). It describes the tilting of the DMSO molecule when the symmetry plane of DMSO is kept in the naphthalene plane. During the vacuum LT calculations  $\beta$  was varied by  $\pm 40^\circ$  in steps of  $2.5^\circ$  starting from the value of  $109.7^\circ$ .
- (3)  **$\delta$  bond length.**  $\delta$  is the length of the intermolecular H bond between the oxygen atom of a DMSO molecule

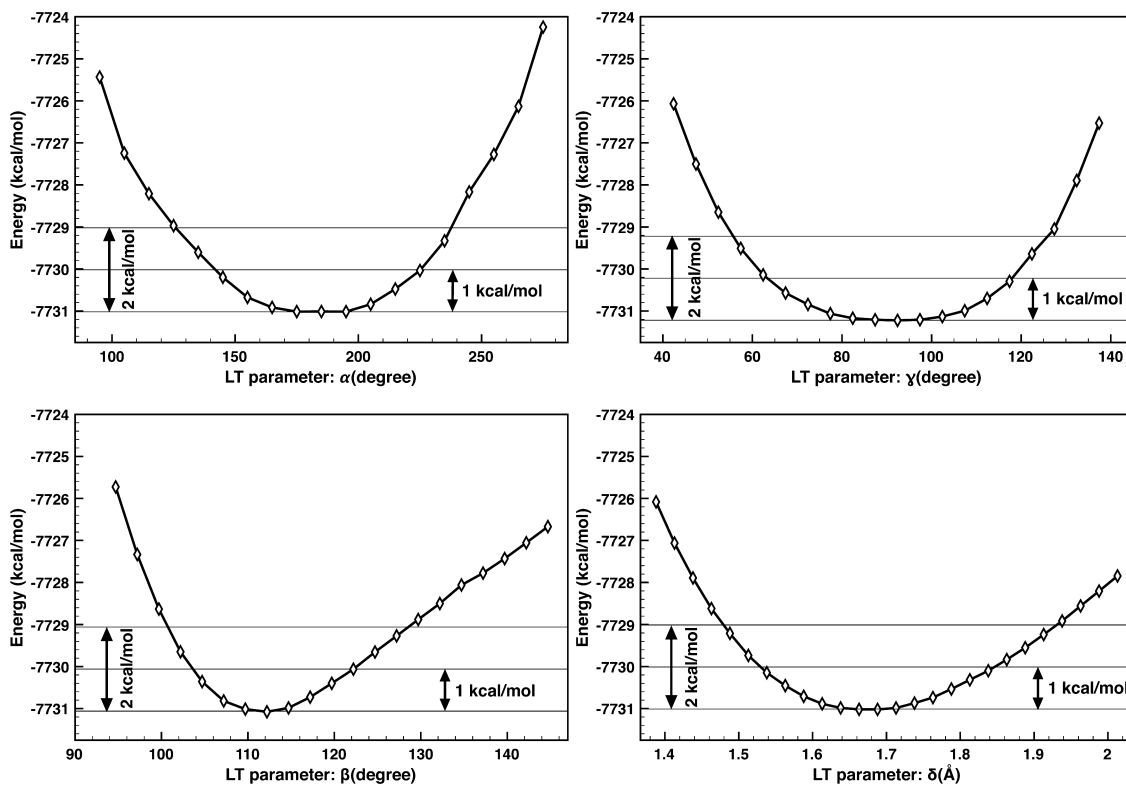


**Figure 3.** Variation of the energy during the LT scans. Four energy plots are shown, i.e., one for each LT parameter.

and the hydrogen atom of an OH group of DBBN (Figure 2). Starting from the value of 1.663 Å,  $\delta$  was varied during the vacuum LT scans by  $\pm 0.275$  Å in steps of 0.025 Å.

- (4) **The  $\gamma$  dihedral angle.**  $\gamma$  is the dihedral angle made by the two naphthalene planes (Figure 2). During the vacuum LT calculations  $\gamma$  was varied by  $\pm 60^\circ$  in steps of  $5^\circ$  starting from  $77^\circ$ . (It should be noted here that although the  $\gamma$  dihedral angle is not associated with the large-amplitude motion of the solvent molecules, variations in  $\gamma$  induce variations in the  $\alpha$  angle that are related to the large-amplitude motion of the solvent. We also note that Bour et al.<sup>36</sup> and Liegeois et al.<sup>37</sup> have carried out investigations similar to our  $\gamma$  LT calculations here for systems very similar to the one considered here.)

Finally, we note that, because the C<sup>3</sup>-(DMSO)<sub>2</sub> complex has C<sub>2</sub> symmetry (like the isolated C<sup>3</sup> conformer), there are two  $\alpha$ , two  $\beta$ , and two  $\delta$  LT parameters (one for each solvent molecule). During the LT scans the LT parameters characterizing the two solvent molecules have been changed simultaneously so that the C<sub>2</sub> symmetry of the C<sup>3</sup>-(DMSO)<sub>2</sub> complex has been preserved.

## 5. RESULTS

**5.1. Analysis of the Vacuum LT Energies.** Figure 3 shows the variation of the energy during the vacuum LT scans for each of the four LT parameters separately. As can be seen, the four energy curves have a rather shallow character (most notably the  $\alpha$  and  $\gamma$  curves), and the variation of the energy during the LT scans is very smooth in all four cases. This shallow character of the energy curves has very important consequences. First, because at room temperature Boltzmann populations may be significant up to an energy of roughly 1 kcal/mol, even relatively large displacements in these coordinates will lead to structures with significant Boltzmann factors. Second, it requires one to perform careful scans of the PES and to investigate the variation of the spectra along the weak intermolecular coordinates; viz., as will be shown in the following sections, slight changes in the relative orientation of the solute and solvent molecules involved in a molecular complex that result in insignificant energy changes can yield very significant changes in the spectra.

**5.2. Analysis of the Vacuum LT Spectra.** Before discussing the similarities and differences observed between the spectra computed for the considered LT structures, it is important to note that only the fingerprint modes in the frequency interval between 1200 and 1700 cm<sup>-1</sup> will be analyzed. The reason is 2-fold. First, due to solvent absorption interference below 1200 cm<sup>-1</sup> experimental spectra are measurable in DMSO solvent only in the region above 1200 cm<sup>-1</sup>. Second, the fingerprint modes in this interval involve variations of molecular parameters that have been fully relaxed during the constrained geometry optimization calculations. As such, the fingerprint modes are predicted accurately<sup>38</sup> by our calculations for the partially optimized LT structures. (Regarding the large-amplitude modes, we note that these modes have frequencies below 100 cm<sup>-1</sup> and are completely decoupled from the fingerprint modes. Furthermore, because the large-amplitude modes involve slow movements of the DMSO molecules with respect to DBBN, they are associated with the weak intermolecular hydrogen bonds that are only partially optimized and therefore cannot be predicted accurately

by our calculations for the partially optimized LT structures.) Figures 4 and 5 show the VA and VCD calculated spectra for all

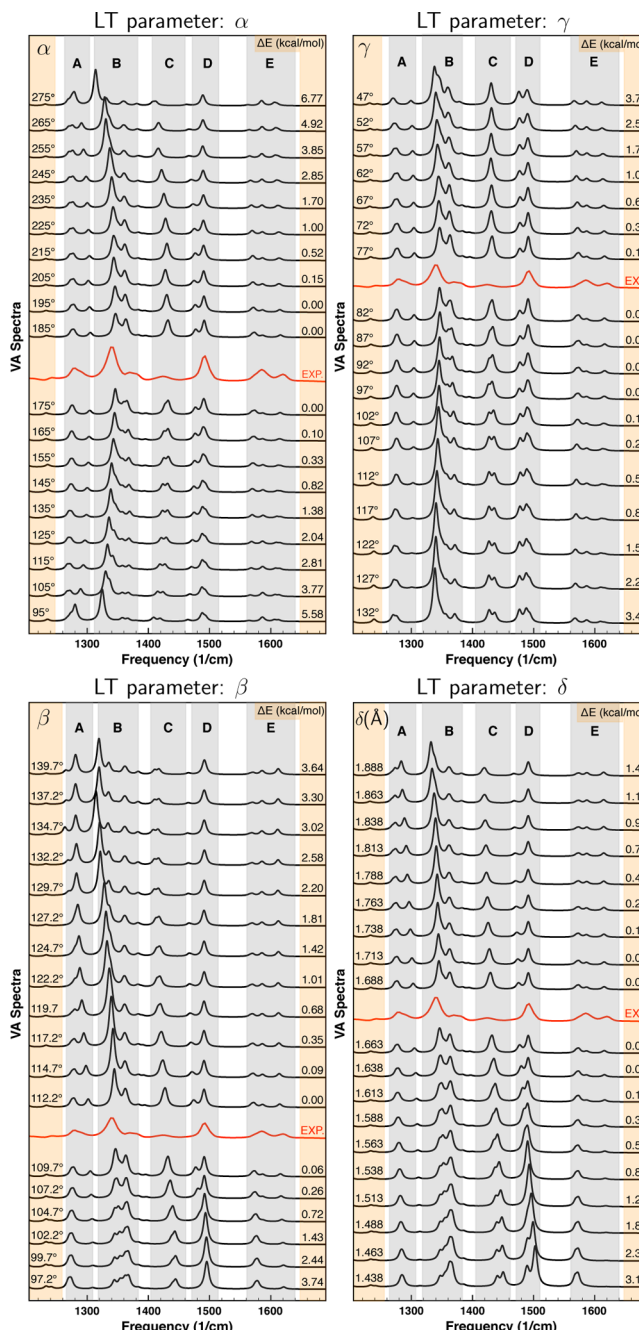


**Figure 4.** Variation of the computed VA spectra during the LT scans. The spectra are grouped into four plots, i.e., one for each LT parameter. Each plot compares the spectra of the LT structures associated with a given LT parameter. The values of the varied LT parameter and the associated relative energy ( $\Delta E$ ) are indicated at each spectrum. The experimental VA and VCD spectra are also shown.

vacuum LT structures. In each figure the spectra are grouped into four different plots, i.e., one for each LT parameter considered. The value of the LT parameter and the relative energy of each LT structure are indicated at each LT spectrum. The experimental VA and VCD spectra are also shown in Figures 4 and 5.

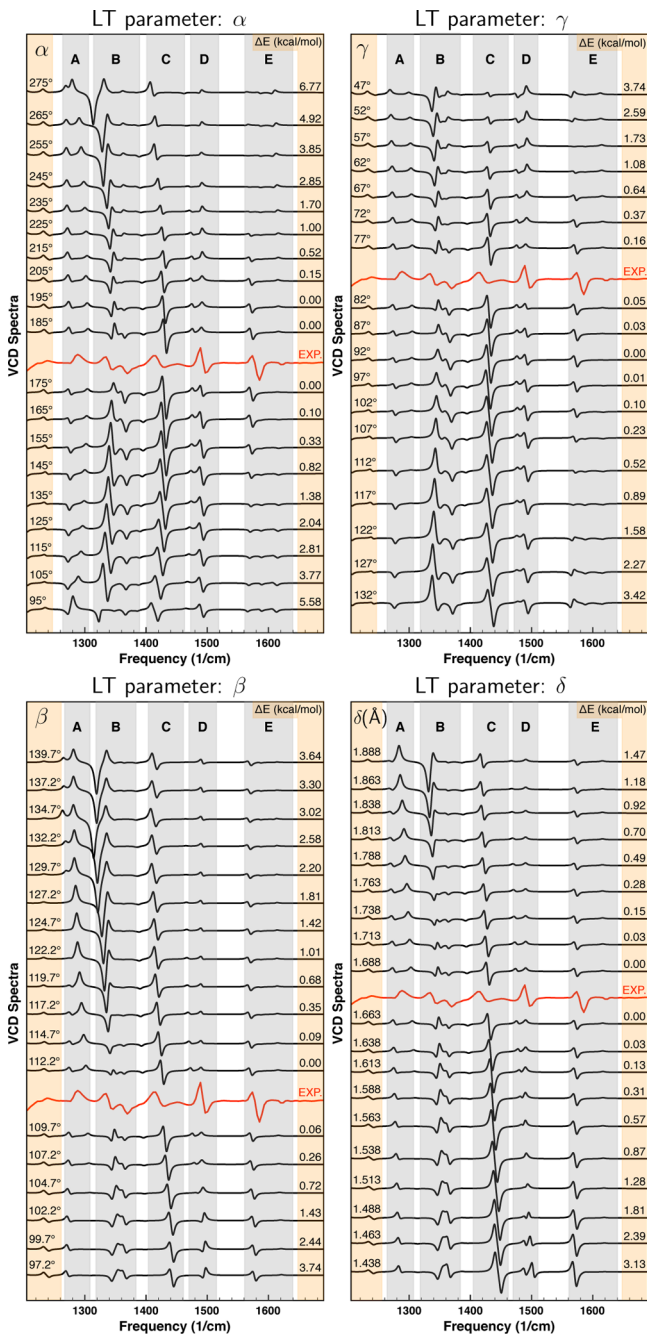


**Figure 5.** Variation of the computed VCD spectra during the LT scans. The spectra are grouped into four plots, i.e., one for each LT parameter. Each plot compares the spectra of the LT structures associated with a given LT parameter. The values of the varied LT parameter and the associated relative energy ( $\Delta E$ ) are indicated at each spectrum. The experimental spectrum (in red) is also shown.

In what follows, we will discuss first (in section 5.2.1) the general trends observed in the LT spectra shown in Figures 4 and 5, then in section 5.2.2 we will look at the effects induced in the spectra by the variation of each LT parameter separately.

**5.2.1. General Trends in the Vacuum LT Spectra.** There are a few main characteristics that are quickly apparent in the LT spectra in Figures 4 and 5:

- (1) The VA and VCD LT spectra of neighboring LT structures exhibit only gradual changes. However, these gradual changes compound and eventually lead to fairly

significant changes in the spectra. This can be seen clearly when spectra of the LT structure with very different values for a given LT parameter are compared.

- (2) For a given LT parameter, the LT structures with the lowest energy (say within 0.5 kcal/mol interval) often have very different VCD spectra in region B. To highlight this, we have used the experimental VCD spectrum (in red) to separate the LT structures that have different VCD spectra. As can be seen in the four plots in Figure 5, in region B the LT VCD spectra situated below the experimental spectrum are very different from the LT VCD spectra situated above the experimental spectrum.

This observation has a very important implication. As can be seen, because of the shallow character of the energy curves in Figure 3, the LT structures with different VCD spectra often have very similar energies; e.g., the energy difference is often smaller than 0.1 kcal/mol. Because such values are smaller than the uncertainty of the computed relative energies, it should be clear that, in situations like this one, it is not recommended to consider a single structure for the solute–solvent molecular complex. (The reason these LT structures, which often are not significantly different, have significantly different VCD spectra will be discussed in section 6.)

- (3) The trends observed in the VA and VCD spectra when  $\gamma$  is varied are often remarkably similar to those obtained when  $\alpha$  is varied. That is, the changes induced in the spectra when  $\gamma$  is varied in one direction are very similar to the changes induced when  $\alpha$  is varied in the opposite direction; e.g., increasing  $\gamma$  is similar to decreasing  $\alpha$ .

This happens because  $\alpha$  and  $\gamma$  LT parameters are correlated to some extent; i.e., when  $\alpha$  is constrained at increasing values, the geometry optimization leads to a decrease in  $\gamma$ , and when  $\gamma$  is constrained at increasing values, the geometry optimization leads to decreasing  $\alpha$  values. As shown in Table 1 in the Supporting Information, during the  $\alpha$  LT scan (i.e., when  $\alpha$  is varied from 90° to 180°)  $\gamma$  varies from 110° to 66°, whereas during the  $\gamma$  LT scans (i.e., when  $\gamma$  is varied from 47° to 137°)  $\alpha$  varies from 201° to 168°.

As will be discussed in section 6, this interconnection between the  $\alpha$  and  $\gamma$  LT parameters has very important consequences for the simulation and interpretation of the VCD spectra.

- (4) The changes observed in the VA and VCD spectra when  $\beta$  is varied in one direction are very similar to those obtained when  $\delta$  is varied in the same direction; e.g., increasing  $\beta$  yields results similar to those obtained when  $\delta$  is increased, though, unlike  $\alpha$  and  $\gamma$ ,  $\beta$  and  $\delta$  are not correlated.

As can be seen, the changes induced in the spectra when  $\beta$  or  $\delta$  is varied are different from those induced when  $\gamma$  or  $\alpha$  is varied.

**5.2.2. Effects Induced in the Spectra by the Variation of the Different LT Parameters.** A detailed analysis of the individual LT spectra in Figures 4 and 5 can be found in section 3 of the Supporting Information. For brevity, in this section we will only assess the overall effects induced in the spectra by the variation of the various LT parameters and whether such variations improve the agreement between the calculated and experimental spectra. To this end, we compare the

experimental spectra to simulated spectra obtained by Boltzmann averaging over the LT spectra associated with a given LT parameter. These simulated spectra, labeled as  $\gamma_{\text{BW}}$ ,  $\alpha_{\text{BW}}$ ,  $\beta_{\text{BW}}$ , and  $\delta_{\text{BW}}$ , are shown in Figure 6.

The VA spectra will be discussed first. As can be seen, overall, the  $\gamma_{\text{BW}}$ ,  $\alpha_{\text{BW}}$ ,  $\beta_{\text{BW}}$ , and  $\delta_{\text{BW}}$  VA spectra are rather similar. However, when looking at details, we see clear differences between them. For example, in the regions A, C, and D the agreement between calculations and experiment is improved when the  $\beta$  and  $\delta$  LT parameters are varied (and not when  $\alpha$

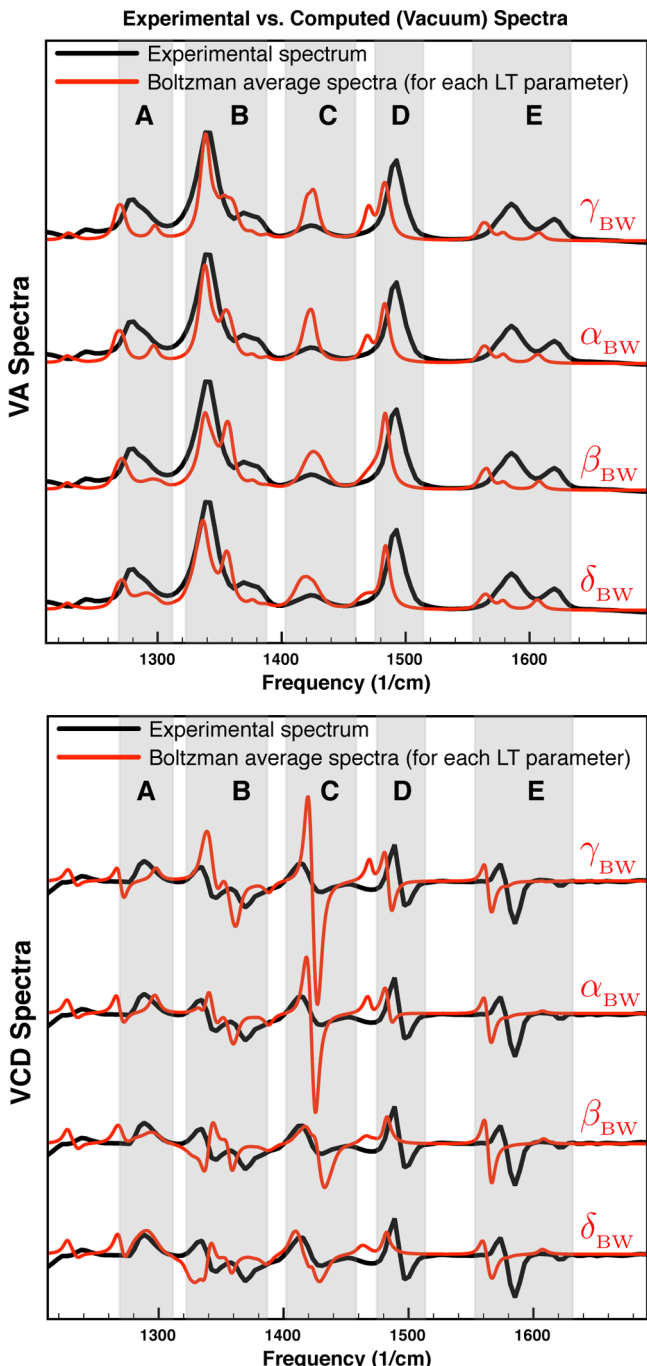


**Figure 6.** Comparison of the VA and VCD experimental spectra to simulated vacuum spectra obtained by Boltzmann averaging the spectra of the vacuum LT structures associated with a given LT parameter.

and  $\gamma$  are varied). In region D, and to a lesser degree also in region A, the agreement with experiment is improved in the  $\beta_{\text{BW}}$  and  $\delta_{\text{BW}}$  spectra because these spectra do not exhibit clear doublet features as the  $\gamma_{\text{BW}}$ ,  $\alpha_{\text{BW}}$  spectra do. Similarly, the  $\beta_{\text{BW}}$  and  $\delta_{\text{BW}}$  VA spectra also reproduce the experimental spectrum better in region C as the band in this region is significantly broader in  $\beta_{\text{BW}}$  and  $\delta_{\text{BW}}$  spectra than in the  $\gamma_{\text{BW}}$ ,  $\alpha_{\text{BW}}$  ones.

In region B, however, the situation is reversed. That is, the agreement with experiment is improved when the  $\gamma$  and  $\alpha$  LT parameters are varied (and not when  $\beta$  and  $\delta$  are varied). The  $\gamma_{\text{BW}}$  spectrum, in particular, reproduces quite well the experiment; viz., it is the only simulated spectrum that does not exhibit a clear doublet feature in this region.

In region E the four simulated VA spectra are rather similar. With respect to the experimental bands, the bands predicted in this region are blue-shifted, have lower intensities, and exhibit a splitting of the left most band into a doublet structure.

Next we look at the VCD spectra (shown in the lower panel of Figure 6). As can be seen, the four simulated VCD spectra show more pronounced differences. In region B, the  $\gamma_{\text{BW}}$  and  $\alpha_{\text{BW}}$  reproduce decently well the  $+/-$  pattern observed in the experimental spectrum, whereas the bands in the  $\beta_{\text{BW}}$  and  $\delta_{\text{BW}}$  spectra seem to have opposite signs compared to peaks in the experimental spectrum. Similarly, in region D, the bisignate  $+/-$  doublet in the experimental spectrum is clearly seen in the  $\gamma_{\text{BW}}$  and  $\alpha_{\text{BW}}$  spectra, but not in the  $\beta_{\text{BW}}$  and  $\delta_{\text{BW}}$  spectra, which exhibit only a positive peak. Because of these differences one can conclude that, unlike in the case of the Boltzmann averaged VA spectra, the  $\gamma_{\text{BW}}$  and  $\alpha_{\text{BW}}$  Boltzmann averaged VCD spectra provide an overall much better description of the experimental spectrum than the  $\beta_{\text{BW}}$  and  $\delta_{\text{BW}}$  Boltzmann averaged VCD spectra.

However, the  $\alpha_{\text{BW}}$  and  $\gamma_{\text{BW}}$  VCD spectra are not overall superior to the  $\beta_{\text{BW}}$  and  $\delta_{\text{BW}}$  ones. As can be seen from the VCD bands in the regions A and C, the  $\beta_{\text{BW}}$  and  $\delta_{\text{BW}}$  spectra capture much better than the  $\gamma_{\text{BW}}$  and  $\alpha_{\text{BW}}$  spectra the relative intensities and the broad character of the experimental bands in these two regions. The  $\delta_{\text{BW}}$  spectrum in particular, reproduces the experimental one very well. The  $\gamma_{\text{BW}}$  and  $\alpha_{\text{BW}}$  spectra, on the other hand, are able to reproduce only the general patterns observed in experiment in regions A and C, i.e., not the broadening of the bands.

In region E, like in the VA spectra, all simulated spectra reproduce the  $+/-$  doublet observed in experiment but exhibit a blue shift of  $10-20 \text{ cm}^{-1}$  (with respect to the experiment).

Based on the analysis performed in Figures 4–6, it is clear that variation of the  $\gamma$  and  $\alpha$  LT parameters is important for improving the agreement with the experimental VA and VCD spectra in the regions B and D, whereas variation of the  $\beta$  and  $\delta$  LT parameters leads to a broadening of the peaks in regions A, C, and D (which improves further, though to a lesser degree, the agreement with experiment). We can therefore conclude that, in the case of the vacuum LT calculations, the most beneficial changes induced in the spectra during the LT scans are those induced when the  $\gamma$  and  $\alpha$  LT parameters are varied; viz., these changes improve significantly the agreement between calculations and experiment in region B.

**5.3. COSMO LT Calculations.** In this section we use the COSMO<sup>30–32</sup> continuum model for solvation to investigate the effects induced in the spectra by the wide solvent environment as a dielectric medium. Although the solvent molecules that interact directly with the solute molecule have evidently to be taken into account explicitly, the use of COSMO may bring

further changes in the computed spectra as it is expected to affect the weak noncovalent bonds between solute molecule and first-sphere solvent molecules.

To investigate these effects, we have performed new geometry optimizations and LT scans (for the same geometrical variables considered in the previous section) for the C<sup>3</sup>-(DMSO)<sub>2</sub> molecular complex embedded in the dielectric continuum corresponding to DMSO (dielectric constant set at 46.7) using the COSMO model. Then, COSMO VA and VCD spectra have been computed for all COSMO LT structures.

Determining an unambiguous equilibrium geometry has proven to be much more difficult in the COSMO calculations than in the vacuum calculations. Because of the shallow energy surfaces and the computational particularities of the COSMO implementation, we could not rely on automatic geometry optimization (not even with the most stringent convergence criteria for the geometry optimization and the highest value for the numerical integration accuracy parameters). That is, to determine the  $\gamma$  and  $\alpha$  values with the lowest energy, it was necessary to perform two-dimensional LT scans in  $\gamma$  and  $\alpha$  (Figure 4, Supporting Information).

The COSMO structures with the lowest energy obtained in this way are significantly different from the vacuum ones. The largest changes are observed for the  $\alpha$  LT parameter (which changed from 160–200° in vacuum to 85–110° in COSMO) and for the  $\gamma$  LT parameter (which changed from 80–110° in vacuum to 70–90° in COSMO). On the other hand, the  $\beta$  and  $\delta$  LT parameters exhibit only minor changes, i.e., less than 10% with respect to the vacuum values. As will be discussed in the end of this section, this shift in the position of the energy minimum has important consequences when the spectra of all COSMO LT structures are Boltzmann averaged.

Figure 7 shows the VA and VCD spectra computed (at COSMO/BP86/TZP level of theory) for the  $\gamma$  and  $\alpha$  COSMO LT parameters obtained by performing two different cuts through the two-dimensional PES (Figure 4, Supporting Information). (The corresponding  $\beta$  and  $\delta$  COSMO LT spectra are shown in Figure 5 in Supporting Information. We note that, like in the case of the vacuum spectra, the variation of the  $\beta$  and  $\delta$  LT parameters leads mostly to a broadening of the COSMO spectra.)

The individual COSMO LT spectra exhibit much the same features as their VACUUM counterparts (compare Figures 4 and 5 with Figure 7 or see Figures 6 and 7 in the Supporting Information for a direct comparison of the vacuum and COSMO spectra). In the case of the VA spectra, the vacuum and COSMO LT spectra exhibit very similar patterns when  $\alpha$  is between 90° and 175° in the  $\alpha$  LT plots, and when  $\gamma$  is between 80° and 136° in the  $\gamma$  LT plots. The most significant differences between the vacuum and COSMO spectra are observed in region D (and to some extent also in region A) where the doublet feature is less obvious in both sets of COSMO spectra. Similar differences are observed also in region B when  $\alpha$  is larger than 175° in the  $\alpha$  LT plots, and when  $\gamma$  is smaller than 80° in the  $\gamma$  LT plots. (These observed differences are expected to lead to a better agreement between the COSMO and experimental spectra.)

Moving to the VCD spectra, we note that, exactly like in the case of the vacuum LT VCD spectra in Figure 5, the COSMO LT structures with the lowest energies often have very different VCD spectra. Also in this case, we have used the experimental VCD spectrum (in red) to separate the LT structures that have different VCD spectra.

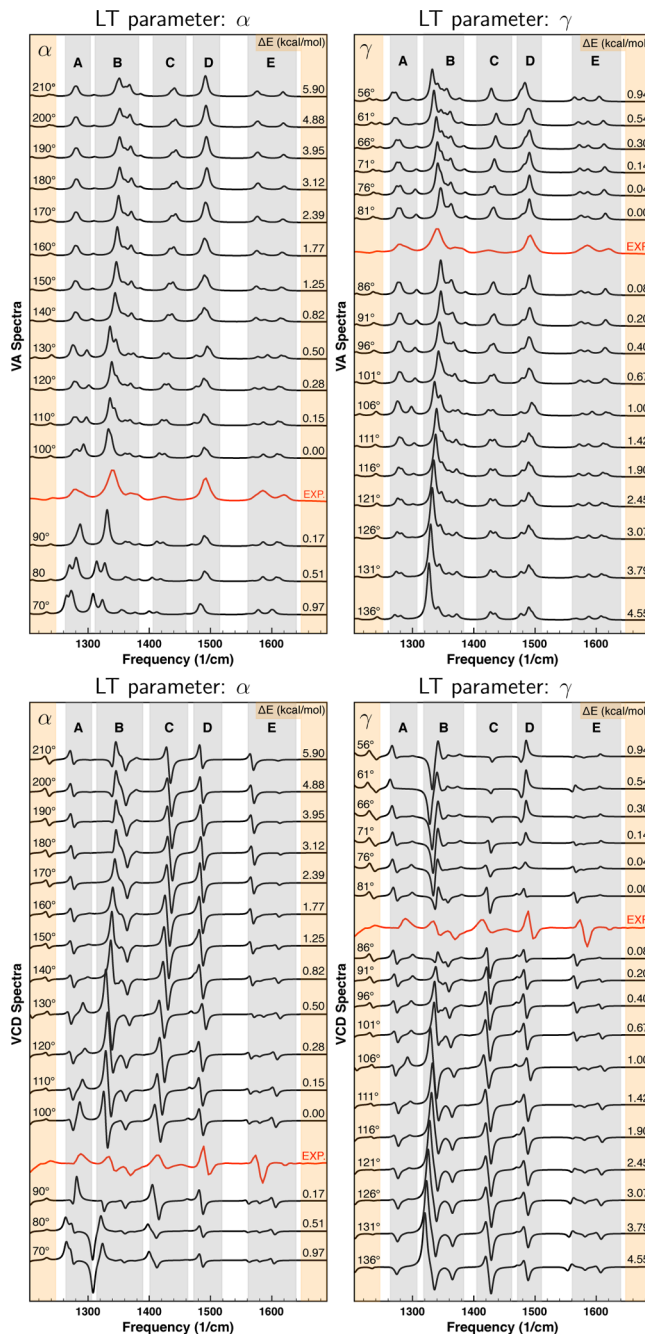


**Figure 7.** VCD and VA spectra computed (at COSMO/BP86/TZP level of theory) for the  $\gamma$  and  $\alpha$  COSMO LT parameters. The spectra are grouped into separate plots, i.e., one for each LT parameter. Each plot compares the spectra of the LT structures associated with a given LT parameter. The values of the varied LT parameter and the associated relative energy ( $\Delta E$ ) are indicated at each spectrum. The experimental spectrum (in red) is also shown.

Looking at the  $\gamma$  LT VCD spectra (Figure 7, Supporting Information), we see that for a given value of the  $\gamma$  LT parameter the patterns observed in the COSMO VCD spectra are remarkably similar to the vacuum ones. On the other hand, the most notable differences between the vacuum and COSMO  $\gamma$  LT spectra are observed in region D, where like in the case of the VA spectra, the COSMO spectra seem to reproduce the experiment a bit better than the vacuum ones.

In the case of the  $\alpha$  LT VCD spectra (Figure 6, Supporting Information), however, one can see clear differences between the patterns in the COSMO and vacuum LT spectra. This is not surprising given the large changes brought about by the use of COSMO in  $\alpha$ . The COSMO VCD spectra of the LT structures with  $\alpha$  between  $90^\circ$  and  $165^\circ$  are very similar to their vacuum counterparts, whereas when  $\alpha$  is larger than  $175^\circ$ , the COSMO and vacuum VCD spectra are very different. As can be seen, the use of COSMO has shifted the position of the energy minimum toward the LT structures that have spectra similar to the experimental ones. As will be shown in Figure 8, this has important consequences when Boltzmann averaging is performed over all LT spectra.

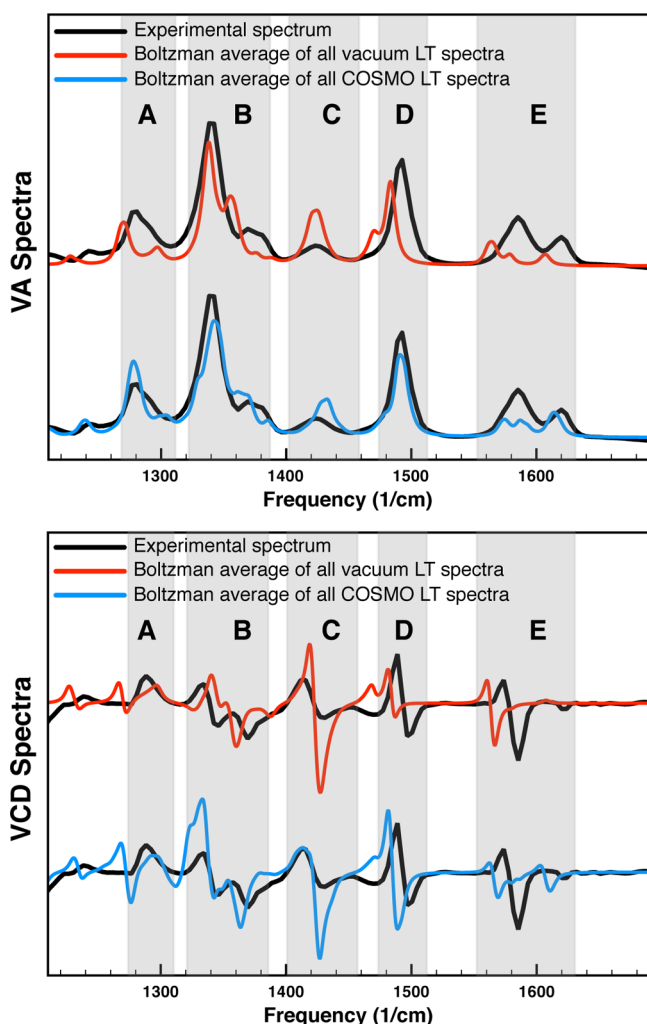


**Figure 8.** Comparison of the VA and VCD experimental spectra to vacuum and COSMO simulated spectra. The simulated spectra have been obtained by Boltzmann averaging the spectra of all LT structures.

Figure 8 shows comparisons between the experimental spectra and the vacuum and COSMO simulated spectra. The simulated spectra have been obtained by Boltzmann averaging the spectra of all LT structures, i.e., all  $\alpha$ ,  $\gamma$ ,  $\beta$ , and  $\delta$  LT structures. As can be seen, both sets of simulated spectra reproduce fairly well the experimental ones. The COSMO spectra provide, however, an overall closer description of the experimental spectra—most notably in region B where the

vacuum VA and VCD simulated spectra provide only a qualitative description of the experimental patterns.

Because, as pointed out earlier, the vacuum and COSMO spectra computed for vacuum and COSMO LT structures that have similar values for  $\alpha$  and  $\gamma$  are very similar, the improvements observed in the COSMO calculations in region B are a direct consequence of the shift in the position of the energy minimum mentioned above; viz., the LT structures that have spectra similar to the experimental spectra have larger Boltzmann factors in the COSMO calculations than in the vacuum ones. This clearly shows that  $\alpha$  (and therefore also  $\gamma$ ) is the most important LT parameters—once  $\alpha$  and  $\gamma$  have the “correct” values, the broad features observed in experiment can be simulated by varying  $\beta$  and  $\delta$ . However, this also suggests that the very difficult COSMO calculations may not be required for finding out what is the most probable relative orientation of the solute and solvent molecules in the experimental sample. That is, this information can be retrieved also from the vacuum calculations (provided that the PES has been thoroughly investigated) by using the experimental spectrum as the reference and the LT spectra (e.g., in Figures 4 and 5) as a map. Of course, more studies are required for confirming this hypothesis.

## 6. NORMAL-MODE ANALYSIS

In this section we discuss the reason for the changes observed in region B in the VCD spectra during the LT scans. Not only are these changes very large, but also, as discussed in the previous sections, to obtain a satisfactory agreement between calculations and experiment, it is crucial for the calculations to reproduce the experimental pattern in this region.

For brevity, but without loss of generality, we will consider here only the changes observed when the  $\alpha$  LT parameter is varied. In Figure 9 we show the patterns in the region B of the VCD spectra of the vacuum LT structures with  $\alpha$  between  $145^\circ$  and  $245^\circ$  and indicate by vertical bars the position and intensity of the normal modes in this region.

To simplify the discussion of the results that will be presented in this section, we will consider the LT structure with  $\alpha = 185^\circ$  as the reference structure for the analysis that will be performed in this section. As can be seen in Figure 9, the VCD spectrum of the LT structure with  $\alpha = 185^\circ$  consists of three intense peaks, that is, a  $-/+$  bisignate feature (determined by modes 126 and 127) followed by a small negative peak (determined by mode 130). When  $\alpha$  decreases during the LT scans, the  $-/+$  bisignate pattern changes sign and becomes  $+/-$ . An increase in the intensity of all three peaks is also observed when  $\alpha$  decreases. On the other hand, when  $\alpha$  increases, the  $-/+$  bisignate pattern becomes more intense but does not change sign, while the peak associated with mode 130 is changing sign.

To monitor how the normal modes in region B change during the LT scans, we have calculated normal-mode overlaps (see refs 15 and 33 for more details) between the modes of the LT structure with  $\alpha = 185^\circ$  in region B and all modes of all  $\alpha$  LT structures. As it turned out, the modes 126 and 127 can be found (almost unaltered) in 11 of the 19  $\alpha$  LT structures. Mode 130, however, does not survive; i.e., the observed VCD sign change for the peak associated with it is caused by mode mixing. Consequently, in what follows only the changes observed for the bisignate feature will be discussed.

Modes 126 and 127 represent a symmetry pair with mode 126 having A symmetry and mode 127 having B symmetry.

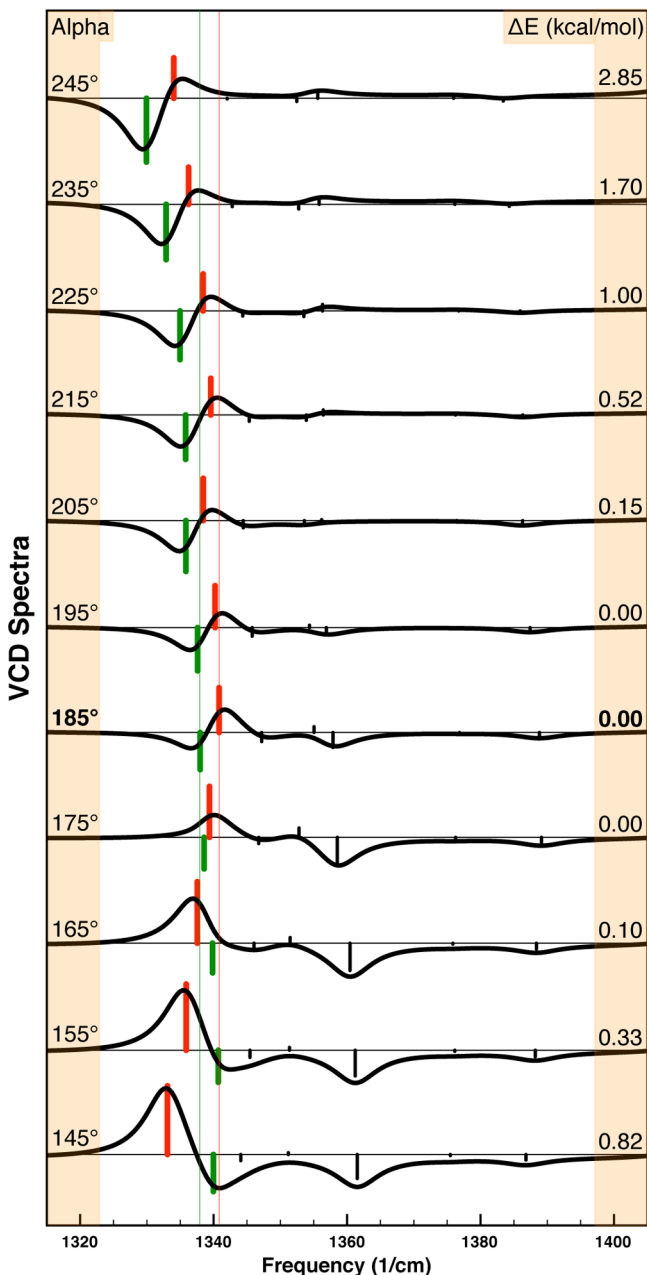


**Figure 9.** Investigation of the sign change observed for the bisignate doublet in region B during the  $\alpha$  LT scan (Figure 5). The vertical bars starting at the baseline of each spectrum indicate the positions and intensities of the rotational strengths of the modes 126 (green) and 127 (red). The thin vertical lines indicate the positions of the modes 126 and 127 in the LT structure with  $\alpha = 185^\circ$ . The value of  $\alpha$  and the relative energy  $\Delta E$  are indicated at each spectrum. Only the spectra of the LT structures listed in Table 2 have been considered.

They are pure DBBN modes that involve a mixture of O–H bendings, in plane C–H bendings and C–C stretchings. The results of the normal-mode analysis performed for these two modes are listed in Table 2. As can be seen, large variations in  $\alpha$  (i.e.,  $40^\circ$  in one direction and  $60^\circ$  in the other direction) that induce large variation in the relative energies of the LT structures (i.e., up to 2.85 kcal/mol) affect very little these normal modes. Indeed, the modes 126 and 127 retain their character during the LT scans and can easily be identified in all  $\alpha$  LT structures listed in Table 2. (The modes 126 and 127 of

**Table 2. Normal-Mode Analysis for the Modes 126 and 127 of the LT Structure with  $\alpha = 185^\circ$  (i.e., the Reference Structure)<sup>a</sup>**

$\alpha$	$\nu$	$\Delta\nu$	$R$	overlap	$\Delta E$
Normal Mode 126 in $\alpha$ LT Structures					
145	1340.0	+2.0	-525.3	0.91	0.82
155	1340.7	+2.7	-445.0	0.95	0.33
165	1339.8	+1.9	-420.9	0.97	0.10
175	1338.6	+0.6	-447.7	0.99	0.00
185	1338.0		-527.6		
195	1337.6	-0.4	-613.9	1.00	0.00
205	1335.9	-2.1	-721.8	0.98	0.15
215	1335.8	-2.2	-630.2	0.99	0.52
225	1335.0	-3.0	-691.6	0.98	1.00
235	1332.9	-5.1	-785.2	0.94	1.70
245	1329.9	-8.0	-905.1	0.90	2.85
Normal Mode 127 in $\alpha$ LT Structures					
145	1333.1	-7.7	+974.4	0.90	0.82
155	1335.9	-4.9	+939.9	0.93	0.33
165	1337.5	-3.3	+872.4	0.96	0.10
175	1339.4	-1.4	+723.8	0.99	0.00
185	1340.8		+635.4		
195	1340.2	-0.6	+594.9	1.00	0.00
205	1338.4	-2.4	+600.4	1.00	0.15
215	1339.6	-1.3	+520.9	0.99	0.52
225	1338.4	-2.4	+525.8	0.99	1.00
235	1336.2	-4.6	+527.7	0.98	1.70
245	1334.0	-6.8	+574.8	0.97	2.85

<sup>a</sup> $\alpha$  is the value of the LT parameter;  $\nu$  is the mode frequency;  $\Delta\nu$  is the variation in frequency with respect to the reference structure;  $R$  is the rotational strength; overlap is the normal-mode overlap;  $\Delta E$  is the relative energy. Units:  $\alpha$  (deg),  $\nu$  ( $\text{cm}^{-1}$ ),  $\Delta\nu$  ( $\text{cm}^{-1}$ ),  $R$  ( $10^{-44} \text{ cm}^2 \text{ esu}^2$ ),  $\Delta E$  (kcal/mol). (The results obtained for the  $\alpha$  LT structures with  $\alpha$  outside the  $145$ – $245^\circ$  interval have not been listed as in those cases the computed normal-mode overlaps are smaller than 0.9.)

the LT structures listed in Table 2 are at least 81% similar to the modes of the reference structure; viz., because two identical modes have an overlap of 1.00, two modes with an overlap 0.9 are 81% similar.) Furthermore, we also note that the largest frequency shift is  $8 \text{ cm}^{-1}$ .

To illustrate the reason for the changes observed in the VCD spectra, the vertical bars associated with the modes 126 and 127 are highlighted in Figure 9 in green and red, respectively. As can be seen, mode 126 has a negative rotational strength while mode 127 has a positive one. In the LT structure with  $\alpha = 185^\circ$  these two modes are very close to each other (less than  $2 \text{ cm}^{-1}$ ). This results in a partial cancellation of their VCD intensities, and therefore to the less intense  $-/+$  feature. For  $\alpha = 175^\circ$  the two modes are almost on top of each other, which leads to a net single weak positive peak in the VCD spectrum—the positive VCD intensity of mode 127 has a larger absolute value than the negative intensity of mode 126, i.e., +635.4 vs -527.6. When  $\alpha$  decreases further (i.e.,  $\alpha < 175^\circ$ ), the two modes interchange their position, as mode 126 exhibits a slight blue shift whereas mode 127 exhibits a slight red shift. As a result, the initial  $-/+$  bisignate feature changes sign and becomes  $+/-$ . When  $\alpha$  increases, on the other hand, both modes shift toward lower frequencies, with mode 126 exhibiting a larger shift. This results in a larger separation between the two modes and no interchange of the mode position. As a result, the initial  $-/+$  bisignate pattern does not change sign and, at the same time, becomes more intense than

in the reference structure (as there is less cancelation between the two peaks of opposite sign).

As this simple normal-mode analysis has shown, the significant changes observed in the VCD spectra in region B are caused by minor perturbations, i.e., very small shifts in the position of two normal modes that have intense VCD intensities. For example, as can be seen in Table 2, when we compare the frequency of the modes 126 and 127 in the reference structure and in the  $\alpha$  LT structure with  $\alpha = 155^\circ$ , a shift of  $2.7 \text{ cm}^{-1}$  in the frequency of mode 126 accompanied by a shift of  $4.7 \text{ cm}^{-1}$  in the opposite direction for the frequency of mode 127 is enough to change the sign of the  $\mp$  bisignate feature.

A more thorough analysis of the  $\alpha$  and  $\gamma$  LT structures has shown that in both vacuum and COSMO calculations the relative position of the modes 126 and 127 is determined mostly by  $\gamma$ . That is, when  $\gamma$  is smaller than a threshold value, the position of the modes 126 and 127 is not interchanged whereas, when  $\gamma$  is larger than the threshold, the position of the two modes is interchanged. This is why in Figures 5 and 7 the VCD LT spectra below the experimental spectrum are significantly different in region B from the VCD LT spectra situated above the experimental one (see also the graphical abstract).

This threshold value for  $\gamma$  depends on the value of  $\alpha$  (i.e., the cut through PES considered) and, as can be seen in Figures 5 and 7, is (slightly) different in the vacuum and COSMO calculations. However, it is interesting to note that most often the  $\gamma$  threshold value is situated very close to the “minimum” of the associated  $\gamma$  energy curve. Therefore, given the very shallow character of the  $\gamma$  energy curves in both vacuum and COSMO calculations and the fact that  $\gamma$  and  $\alpha$  LT parameters are interconnected, it is clear that, to make reliable predictions, one needs to take into account the effect of the spectrum variation along the  $\gamma$  and  $\alpha$  coordinates.

Finally, we note that the simple mechanism uncovered in this section is responsible also for the sign change observed in the vacuum  $\gamma$  LT spectra in region D; i.e., like in region B, what we observe in region D is not an actual sign change, but merely an interchange of the position of two neighboring modes that have opposite VCD signs.

We can therefore conclude that the analysis performed in this section has provided a very simple and intuitive explanation for the observations made in the previous sections; i.e., moderate displacements along a LT coordinate (that result in insignificant changes in energy) may yield very different VCD patterns in some regions of the spectrum. Furthermore, as already mentioned, this analysis has also demonstrated the need to perform linear transit calculations in situations like this one.

## 7. CONCLUSION

Using as examples the VA and VCD spectra of the 6,6'-dibromo-[1,1'-binaphthalene]-2,2'-diol molecule measured in DMSO, in this study we have investigated the effects induced in the VA and VCD spectra by the large-amplitude motion of the solvent molecules loosely bound to the solvent. To this end, a benchmark study was performed by systematically varying the relative orientation and position of the solute and solvent molecules (by performing linear transit calculations) and computing vacuum and COSMO VA and VCD spectra for all generated linear transit structures. This investigation has shown the following:

- (1) The large-amplitude motions can induce very significant changes in the VA and VCD spectra.
- (2) The importance of investigating the variation of the spectra along the weak intermolecular coordinates. As shown in section 6, slight changes in the relative orientation of the solute and solvent molecules involved in a molecular complex (that induce insignificant energy changes) may lead to very significant changes in the VCD spectra. We stress that such minor geometrical changes can easily be caused by small changes in the computational settings, e.g., basis sets, convergence criteria, and even the structure used as starting point in the geometry optimization calculations. Therefore, making a prediction based on calculations performed for a single structure of the solute–solvent molecular complex is not recommended.
- (3) The changes induced in the VA and VCD spectra by large-amplitude motions can be simulated by performing linear transit scans and obtaining the computed spectra as Boltzmann averages over all linear transit structures.
- (4) Using continuum solvation models like COSMO is important when one is simulating spectra of molecular complexes formed via weak intermolecular hydrogen bonds. As discussed in section 5.3, although the vacuum and COSMO spectra computed for vacuum and COSMO LT structures that have similar geometrical parameters are quite similar, the use of COSMO has shifted the minimum of the energy curves toward the linear transit structures whose spectra resembled the experimental spectra. As a result, the COSMO Boltzmann weighted spectra reproduces the experimental spectra better than the vacuum ones.

Further, we note that the linear transit calculations performed here have also provided an explanation for the broader character of the experimental bands in the  $1200\text{--}1450 \text{ cm}^{-1}$  region. This feature is often observed in experimental spectra measured in hydrogen bonding solvents<sup>10,39,40</sup> (generally for O–H containing molecules), but it is not explained in the literature.

Finally, we note that, because the variation of the different LT parameters improves the agreement with experiment in different frequency regions (see section 5.2.2 and section 3 in the Supporting Information), by using the experimental spectrum as a reference, one could in principle use the comparisons of the individual LT spectra in Figures 4 and 5 as a map for determining the most probable values in the experimental sample of the geometrical parameters describing the relative orientation of the solute and solvent molecules involved in the molecular complex. This suggests that VCD spectroscopy could provide key information for elucidating the role played by the solvent in asymmetric synthesis and catalysis—a crucial step for understanding the mechanisms behind such reactions.

In closing, we note that, for solvents that do not participate in hydrogen bonding with the solute, it may not be necessary to take into account the effects induced in the spectra by these large-amplitude motions—it is cumbersome to take this effect into account. However, in solvents that participate in hydrogen bonding (e.g., DMSO), and especially in molecular systems characterized by one or more weak coordinates that can easily be affected by the weak H intermolecular bonds formed between solute and solvent (think at the  $\gamma$  and  $\alpha$  coordinates in

the present study), it may be necessary to perform such a sampling of the configurational space, viz. to eliminate uncertainties about the assignment of absolute configuration and to minimize the discrepancies between experiment and calculation.

## ASSOCIATED CONTENT

### Supporting Information

Vacuum and COSMO VA and VCD spectra of the isolated conformers;  $\alpha$  values for the  $\gamma$  LT structures;  $\gamma$  values for the  $\alpha$  LT structures parameters; COSMO  $\gamma\alpha$  PES; COSMO  $\beta$  and  $\delta$  VA and VCD spectra; analysis of all vacuum LT spectra;  $\alpha$  and  $\gamma$  VA and VCD spectra; vacuum vs COSMO calculations. This material is available free of charge via the Internet at <http://pubs.acs.org>

## AUTHOR INFORMATION

### Corresponding Author

\*V. P. Nicu: e-mail, v.p.nicu@vu.nl, vp.nicu@gmail.com.

### Notes

The authors declare no competing financial interest.

## ACKNOWLEDGMENTS

This work was supported by The Netherlands' Foundation for Scientific Research (VENI grant V.P.N.), by the National Research School combination "Catalysis by Design" (M.H.) and by the WCU (World Class University) program (E.J.B.) through the Korea Science and Engineering Foundation funded by the Ministry of Education, Science, and Technology of the Republic of Korea (Project No. R32-2008-000-10180-0). Funding from NSF (CHE-0804301) is gratefully acknowledged by P.L.P. We are also grateful for computational time granted by The Netherlands' Foundation for Scientific Research via its EW branch.

## REFERENCES

- (1) Aydin, J.; Kumar, K. S.; Sayah, M. J.; Wallner, O. A.; Szabo, K. J. Synthesis and Catalytic Application of Chiral 1,1'-Bi-2-Naphthol- and Biphenanthrol-Based Pincer Complexes: Selective Allylation of Sulfonimines with Allyl Stannane and Allyl Trifluoroborate. *J. Org. Chem.* **2007**, *72*, 4689–4697.
- (2) Paton, R. S.; Goodman, J. M.; Pellegrinet, S. C. Theoretical Study of the Asymmetric Conjugate Alkenylation of Enones Catalyzed by Binaphthols. *J. Org. Chem.* **2008**, *73*, 5078–5089.
- (3) Noyori, R.; Takaya, H. Binaphthyls: The Beauty and Chiral Uses. *J. Chem. Scripta* **1985**, *25*, 83–89.
- (4) Lin, M.; Kang, G.; Guo, Y.; Yu, Z. X. Asymmetric Rh(I)-Catalyzed Intramolecular [3 + 2] Cycloaddition of 1-Yne-Vinylcyclopropanes for Bicyclo[3.3.0] Compounds with a Chiral Quaternary Carbon Stereocenter and Density Functional Theory Study of the Origins of Enantioselectivity. *J. Am. Chem. Soc.* **2012**, *134*, 398–405.
- (5) Wynberg, H.; Greijdanus, B. Solvent Effects in Homogeneous Asymmetric Catalysis. *J. Chem. Soc., Chem. Commun.* **1978**, *10*, 427–428.
- (6) Sohtome, Y.; Nagasawa, K. Dynamic Asymmetric Organocatalysis: Cooperative Effects of Weak Interactions and Conformational Flexibility in Asymmetric Organocatalysts. *Chem. Commun.* **2012**, *48*, 7777–7789.
- (7) Cainelli, G.; Galletti, P.; Giacomini, D. Solvent Effects on Etereoselectivity: more than just an Environment. *Chem. Soc. Rev.* **2009**, *38*, 990–1001.
- (8) Wang, F.; Polavarapu, P. L.; Schurug, V.; Schmidt, R. Absolute Configuration and Conformational Analysis of a Degradation Product of Inhalation Anesthetic Sevoflurane: A Vibrational Circular Dichroism Study. *Chirality* **2002**, *14*, 618–624.
- (9) Yang, G.; Xu, Y. The Effects of Self-Aggregation on the Vibrational Circular Dichroism and Optical Rotation Measurements of Glycidol. *Phys. Chem. Chem. Phys.* **2008**, *10*, 6787–6795.
- (10) Nicu, V. P.; Baerends, E. J.; Polavarapu, P. L. Understanding Solvent Effects in Vibrational Circular Dichroism Spectra: [1,1'-Binaphthalene]-2,2'-Diol in Dichloromethane, Acetonitrile, and Dimethyl Sulfoxide Solvents. *J. Phys. Chem. A* **2012**, *116*, 8366–8373.
- (11) Kuppens, T.; Herrebout, W.; van der Veken, B.; Bultinck, P. Intermolecular Association of Tetrahydrofuran-2-Carboxylic Acid in Solution: A Vibrational Circular Dichroism Study. *J. Phys. Chem. A* **2006**, *110*, 10191–10200.
- (12) Debie, E.; Bultinck, P.; Herreboutand, W.; van der Veken, B. Solvent Effects on IR and VCD Spectra of Natural Products: an Experimental and Theoretical VCD Study of Pulegone. *Phys. Chem. Chem. Phys.* **2008**, *10*, 3498–3508.
- (13) Losada, M.; Tran, H.; Xu, Y. Lactic Acid in Solution: Investigations of Lactic Acid Self-Aggregation and Hydrogen Bonding Interactions with Water and Methanol Using Vibrational Absorption and Vibrational Circular Dichroism Spectroscopies. *J. Chem. Phys.* **2008**, *128*, 014508.
- (14) Nicu, V. P.; Autschbach, J.; Baerends, E. J. Enhancement of IR and VCD Intensities due to Charge Transfer. *Phys. Chem. Chem. Phys.* **2009**, *11*, 1526–1538.
- (15) Nicu, V. P.; Debie, E.; Herrebout, W.; Veken, B. V. D.; Bultinck, P.; Baerends, E. J. A VCD Robust Mode Analysis of Induced Chirality: The Case of Pulegone in Chloroform. *Chirality* **2010**, *21*, E287–E297.
- (16) Liu, Y.; Yang, G.; Losada, M.; Xu, Y. Vibrational Absorption, Vibrational Circular Dichroism, and Theoretical Studies of Methyl Lactate Self-Aggregation and Methyl Lactate-Methanol Intermolecular Interactions. *J. Chem. Phys.* **2010**, *132*, 234513.
- (17) Goncharova, I.; Sykora, D.; Urbanova, M. Association of Biotin with Silver (I) in Solution: a Circular Dichroism Study. *Tetrahedron: Asymmetry* **2010**, *21*, 1916–1920.
- (18) Nicu, V.; Heshmat, M.; Baerends, E. J. Signatures of Counter-Ion Association and Hydrogen Bonding in Vibrational Circular Dichroism Spectra. *Phys. Chem. Chem. Phys.* **2011**, *13*, 8811–8825.
- (19) Gobi, S.; Vass, E.; Magyarfalvi, G.; Tarczay, G. Effects of Strong and Weak Hydrogen Bond Formation on VCD Spectra: a Case Study of 2-Chloropropionic Acid. *Phys. Chem. Chem. Phys.* **2011**, *13*, 13972–13984.
- (20) Merten, C.; Amkreutz, M.; Hartwig, A. Determining the Structure of  $\alpha$ -Phenylethyl Isocyanide in Chloroform by VCD Spectroscopy and DFT Calculations – Simple Case or Challenge? *Phys. Chem. Chem. Phys.* **2010**, *12*, 11635–11641.
- (21) Zamfir, A.; Schenker, S.; Freund, M.; Tsogoeva, S. B. Chiral BINOL-Derived Phosphoric Acids: Privileged Brønsted Acid Organocatalysts for CC Bond Formation Reactions. *Org. Biomol. Chem.* **2010**, *8*, 5262–5276.
- (22) Shanmugam, G.; Polavarapu, P. L. Vibrational Circular Dichroism of Protein Films. *J. Am. Chem. Soc.* **2004**, *126*, 10292–10295.
- (23) Amsterdam Density Functional Program. Theoretical Chemistry, Vrije Universiteit, Amsterdam, URL: <http://www.scm.com>.
- (24) Velde, G. T.; Bickelhaupt, F. M.; Baerends, E. J.; Guerra, C. F.; Gisbergen, S. J. A. V.; Snijders, J. G.; Ziegler, T. Chemistry with ADF. *J. Comput. Chem.* **2001**, *22*, 931–967.
- (25) Guerra, C. F.; Snijders, J.; te Velde, G.; Baerends, E. Towards an Order-N DFT Method. *Theor. Chem. Acc.* **1998**, *99*, 391–403.
- (26) Nicu, V. P.; Neugebauer, J.; Wolff, S. K.; Baerends, E. J. A Vibrational Circular Dichroism Implementation within a Slater-type-Orbital Based Density Functional Framework and its Application to Hexa- and Hepta-Helicenes. *Theor. Chem. Acc.* **2008**, *119* (1–3), 245–263.
- (27) Perdew, J. P. Density-functional approximation for the correlation energy of the inhomogeneous electron gas. *Phys. Rev. B* **1986**, *33*, 8822–8824.
- (28) Becke, A. D. Density-Functional Exchange-Energy Approximation with Correct Asymptotic Behavior. *Phys. Rev. A* **1988**, *38*, 3098–3100.

- (29) van Lenthe, E.; Baerends, E. Optimized Slater-Type Basis Sets for Elements 1–118. *J. Comput. Chem.* **2003**, *24*, 1142–1156.
- (30) Klamt, A.; Schüürmann, G. COSMO: a New Approach to Dielectric Screening in Solvents with Explicit Expressions for the Screening Energy and its Gradient. *J. Chem. Soc., Perkin Trans. 2* **1993**, 799–805.
- (31) Klamt, A. Conductor-like Screening Model for Real Solvents: A New Approach to the Quantitative Calculation of Solvation Phenomena. *J. Phys. Chem.* **1995**, *99*, 2224–2235.
- (32) Klamt, A.; Jones, V. Treatment of the Outlying Charge in Continuum Solvation Models. *J. Chem. Phys.* **1996**, *105*, 9972–9981.
- (33) Nicu, V. P.; Neugebauer, J.; Baerends, E. J. Effects of Complex Formation on Vibrational Circular Dichroism Spectra. *J. Phys. Chem. A* **2008**, *112* (30), 6978–6991.
- (34) Sahnoun, R.; Koseki, S.; Fujimura, Y. Theoretical Investigation of 1,1'-Bi-2-Naphthol Isomerization. *J. Mol. Struct.* **2005**, *735*–736, 315–324.
- (35) Polavarapu, P. L.; Jeirath, N.; Walia, S. Conformational Sensitivity of Chiroptical Spectroscopic Methods: 6,6'-Dibromo-1,1'-Bi-2-Naphthol. *J. Phys. Chem. A* **2009**, *113*, 5423–5431.
- (36) Setnicka, V.; Urbanova, M.; Bour, P.; Kral, V.; Volka, K. Vibrational Circular Dichroism of 1,1'Binaphthyl Derivatives: Experimental and Theoretical Study. *J. Phys. Chem. A* **2001**, *105*, 8931–8938.
- (37) Liegeois, V. A Vibrational Raman Optical Activity Study of 1,1'-Binaphthyl Derivatives. *ChemPhysChem* **2009**, *10*, 2017–2025.
- (38) Banks, S. T.; Clary, D. C. Chemical Reaction Surface Vibrational Frequencies Evaluated in Curvilinear Internal Coordinates: Application to  $\text{H} + \text{CH}_4 \rightleftharpoons \text{H}_2 + \text{CH}_3$ . *J. Chem. Phys.* **2009**, *130*, 024106.
- (39) Losada, M.; Xu, Y. Chirality Transfer Through Hydrogen-Bonding: Experimental and Ab Initio Analyses of Vibrational Circular Dichroism Spectra of Methyl Lactate in Water. *Phys. Chem. Chem. Phys.* **2007**, *9*, 3127–3135.
- (40) Poopari, M. R.; Dezhahang, Z.; Xu, Y. A Comparative VCD Study of Methyl Mandelate in Methanol, Dimethyl Sulfoxide, and Chloroform: Explicit and Implicit Solvation Models. *Phys. Chem. Chem. Phys.* **2013**, *15*, 1655–1665.